Microstructural Evolution During Cold Rolling and Subsequent Annealing in Low-Carbon Steel with Different Initial Microstructures

Toshio Ogawa, Hiroyuki Dannoshita, Kuniaki Maruoka, and Kohsaku Ushioda

Microstructural evolution during cold rolling and subsequent annealing of low-carbon steel with different initial microstructures was investigated from the perspective of the competitive phenomenon between recrystallization of ferrite and reverse phase transformation from ferrite to austenite. Three kinds of hot-rolled sheet specimens were prepared. Specimen P consisted of ferrite and pearlite, specimen B consisted of bainite, and specimen M consisted of martensite. The progress of recovery and recrystallization of ferrite during annealing was more rapid in specimen M than that in specimens P and B. In particular, the recrystallized ferrite grains in specimen M were fine and equiaxed. The progress of ferrite-to-austenite phase transformation during intercritical annealing was more rapid in specimen M than in specimens P and B. In all specimens, the austenite nucleation sites were mainly at high-angle grain boundaries, such as those between recrystallized ferrite grains. The austenite distribution was the most uniform in specimen M. Thus, we concluded that fine equiaxed recrystallized ferrite grains were formed in specimen M, leading to a uniform distribution of austenite.

1. Introduction

Low-carbon steels used in the automobile industry are generally manufactured by continuous casting, hot rolling, cold rolling, and annealing. The microstructure of such sheets depends strongly on the manufacturing conditions. Thus, it is necessary to establish a method of microstructural control by optimizing the manufacturing process.

It has been reported that the grain size of hot-rolled sheets can affect the recrystallization of ferrite during annealing in interstitial-free (IF) steel and pure iron (Ref 1-3). For instance, Abe et al. (Ref 1) reported that grain refinement in hot-rolled sheets leads to the formation of a γ-fiber (ND//<111>) texture, where ND stands for the direction normal to the sheet plane. In the case of low-carbon steel, it has been demonstrated that the initial microstructure before cold rolling can affect microstructural evolution during annealing and the mechanical properties after annealing (Ref 4-6). In previous studies, the influence of the microstructure prior to cold rolling on recrystallization (Ref 4) and formation of retained austenite

(Ref 5) has been discussed. Karmakar et al. (Ref 6) investigated the influence of the initial microstructure on microstructural evolution during intercritical annealing. However, they did not sufficiently address competition between recrystallization and the ferrite-to-austenite phase transformation. Moreover, detailed research has yet to be conducted on the influence of the initial microstructure on recovery during annealing. Therefore, the effects of the initial microstructure on competition among recovery, recrystallization, and the ferrite-to-austenite phase transformation during annealing remain unclear.

It has been demonstrated that microstructural evolution during annealing of low-carbon steel is very complicated since several metallurgical phenomena, such as recovery, recrystallization and ferrite-to-austenite phase transformation, occur simultaneously (Ref 7-10). Furthermore, it has been reported that grain refinement and good formability can be achieved by controlling the initial microstructure (Ref 11, 12). Thus, for precise control of the mechanical properties, it is necessary to characterize the competition among recovery, recrystallization, and the ferrite-to-austenite phase transformation during annealing of low-carbon steel with different initial microstructures. The purpose of the present study is to clarify these competitive processes during cold rolling and annealing of low-carbon steel.

2. Materials and Methods

The chemical composition of the tested low-carbon steel with 0.10 mass% C and 2.00 mass% Mn given in Table 1 is based on our previous studies (Ref 7, 8). The addition of Mn increases the hardenability of the tested steel. The vacuum-melted ingots (approximately $100 \times 100 \times 500$ mm) were rough rolled to a thickness of 30 mm. The rough rolled steels were hot rolled at a finishing temperature of 900 °C in the austenite region to a thickness of 3.0 mm, and subsequently

Toshio Ogawa, Hiroyuki Dannoshita, and Kuniaki Maruoka, Department of Mechanical Engineering, National Institute of Technology, Kisarazu College, 2-11-1 Kiyomidai-higashi, Kisarazu, Chiba 292-0041, Japan; and Kohsaku Ushioda, Graduate School of Natural Science and Technology, Kanazawa University, Kakuma-machi, Kanazawa, Ishikawa 920-1192, Japan and Technical Research and Development Bureau, Nippon Steel & Sumitomo Metal Corporation, 20-1 Shintomi, Futtsu, Chiba 293-8511, Japan. Contact e-mail: ogawa@m.kisarazu.ac.jp.

water cooled to 650 °C (specimen P), 500 °C (specimen B) and below 100 °C (specimen M). The microstructure of each of these hot-rolled sheet specimens is shown in Fig. 1. Specimen P consisted of ferrite and pearlite (Fig. 1a), specimen B consisted of bainite (Fig. 1b), and specimen M consisted of martensite (Fig. 1c). The hot-rolled sheets were cold-rolled to a thickness of 1.0 mm (reduction: 67%) by four-high cold rolling mill at a rolling speed of 15 m/min. The microstructure of each cold-rolled sheet specimen is shown in Fig. 2.

The cold-rolled sheets were cut into 1.0 (thickness) $\times$ 10 $\times$ 10 mm specimens. The specimens were heated to the target temperature at a rate of 0.5 °C/s using an electric furnace, and then water quenched to room temperature. The Ac_1 temperature of the tested steel is approximately 670 °C. During the cooling process, the austenite phase, which was present during intercritical annealing, transformed into martensite.

The microstructures of nital-etched specimens were observed by optical microscopy and scanning electron microscopy (SEM). Vickers hardness tests were conducted ($n = 3$) under an applied load of 19.6 N for 10 s to estimate the recrystallized fraction, F_R, using the Eq 1 (Ref 13):

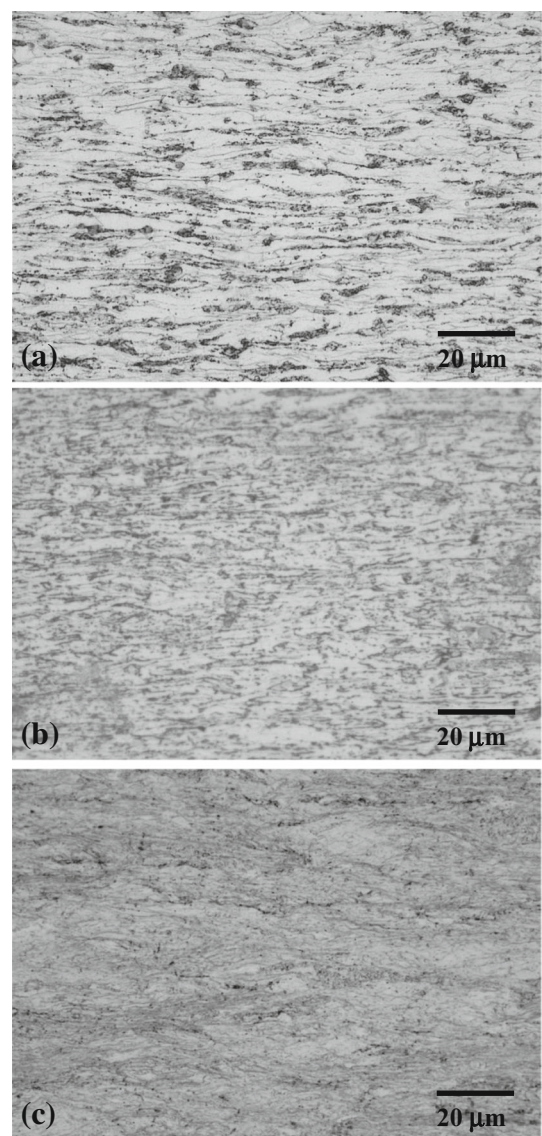$$F_R = \frac{H_{NR} - H_w}{H_{NR} - H_R} \times 100 \qquad \text{(Eq 1)}$$

where H_w is the Vickers hardness of the entire specimen, H_{NR} is the Vickers hardness of the as-cold rolled specimen,

Table 1 Chemical composition of the steel used in the present study (mass%)

C	Si	Mn	P	S	Al	N
0.10	0.010	2.00	0.010	0.0030	0.030	0.0030
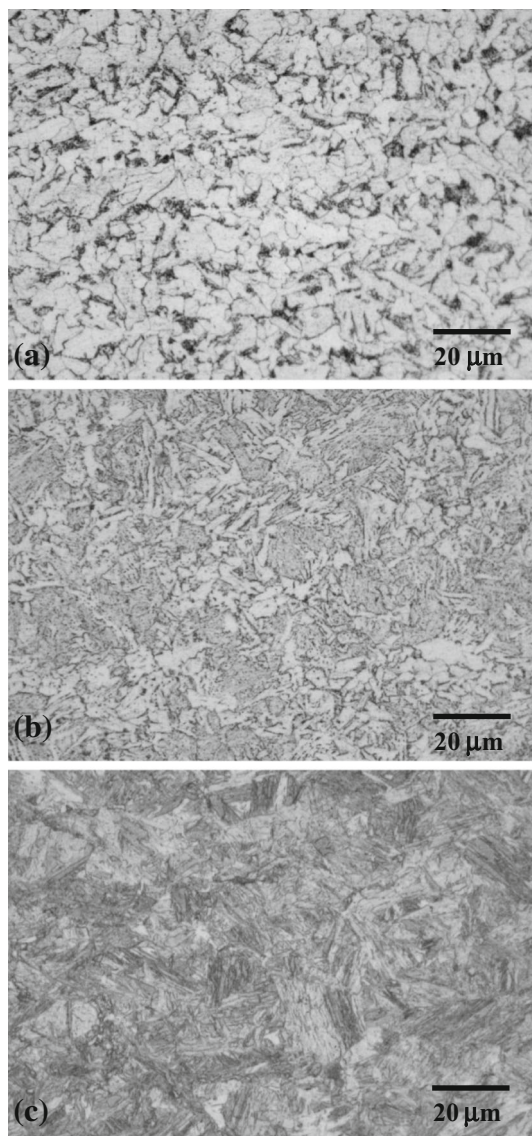
Fig. 1 Microstructure of hot-rolled sheets of specimens (a) P, (b) B, and (c) M

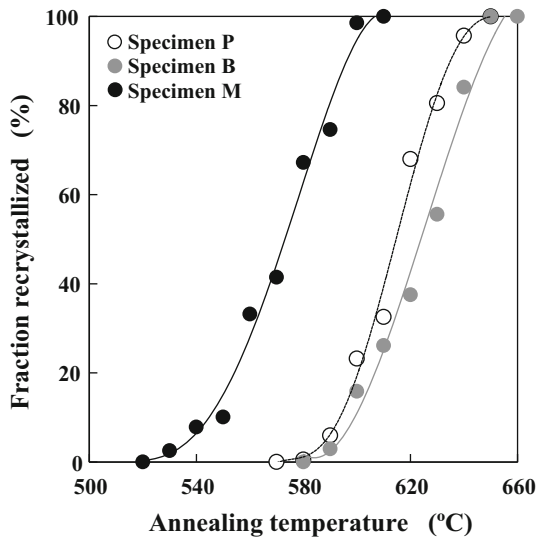Fig. 2 Microstructure of cold-rolled sheets of specimens (a) P, (b) B, and (c) M

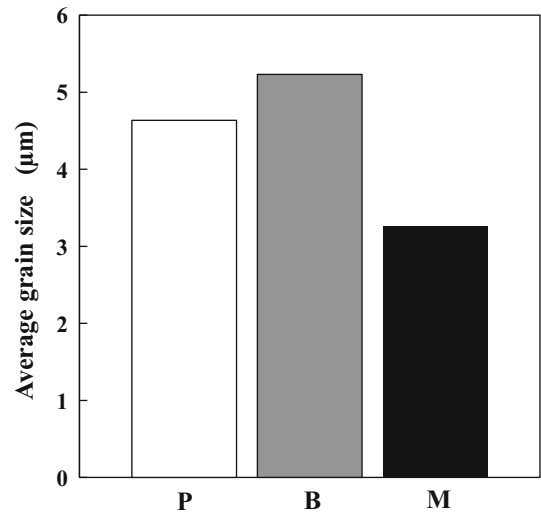**Fig. 3** Recrystallized fraction as function of annealing temperature

Fig. 5 Grain size for recrystallized ferrite in specimens P, B, and M, immediately after completion of ferrite recrystallization
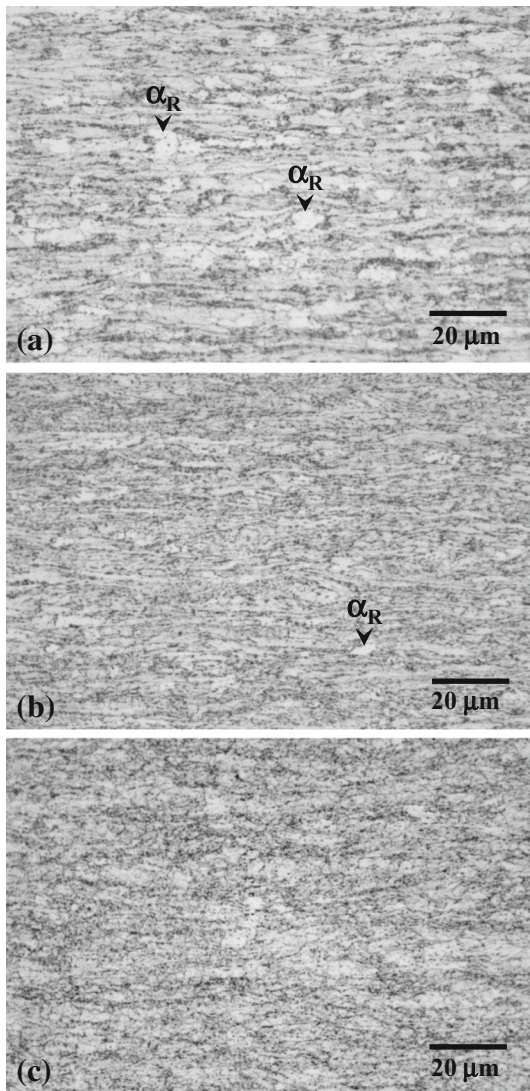
and H_R is the Vickers hardness of the fully recrystallized specimen. F_R is rigorously an index of fraction softened; however, in the present study it is used as an index of fraction recrystallized for the sake of simplicity. A decrease in hardness during annealing in the single-phase ferrite region is mainly attributed to progress of ferrite recrystallization. In the Eq 1, since H_{NR} and H_R are constant values in each specimen, F_R increases with decreasing H_w. For instance, if H_w equals H_{NR}, namely, immediately before the start of ferrite recrystallization, F_R is calculated to be 0% by using the Eq 1. In addition, if H_w equals H_R, namely, immediately after the completion of ferrite recrystallization, F_R is calculated to be 100% by using the Eq 1. The fraction of martensite was estimated by the point-count method (ASTM E 562). The estimated martensite fraction corresponds to the fraction of austenite during intercritical annealing since the austenite transforms into martensite during the cooling process. In addition, the recrystallized ferrite grain size and the distance between martensite regions were measured from the SEM images. The recrystallized ferrite grain size was determined based on ASTM E 112. The number of samples of distance between martensite regions was 200 in each specimen.

Microtexture analysis was carried out using an EBSD/FEGSEM system employing OIM software on the rolling plane with annealed specimens at the quarter-thickness position (distance from the surface is approximately 0.25 mm). The step size of the EBSD measurements was 0.2 μm.

3. Results

3.1 Microstructural Evolution During Annealing in the Single-Phase Ferrite Region

Figure 3 shows the variation in the recrystallized fraction for each specimen during annealing. Clearly, the starting temperature for ferrite recrystallization was markedly lower for specimen M than for specimens P and B. In addition, the starting temperature for ferrite recrystallization for specimen P was slightly lower than that for specimen B. The microstructure

Fig. 4 Microstructure of specimens (a) P, (b) B, and (c) M, heated to 610 °C (α_R: recrystallized ferrite grains)
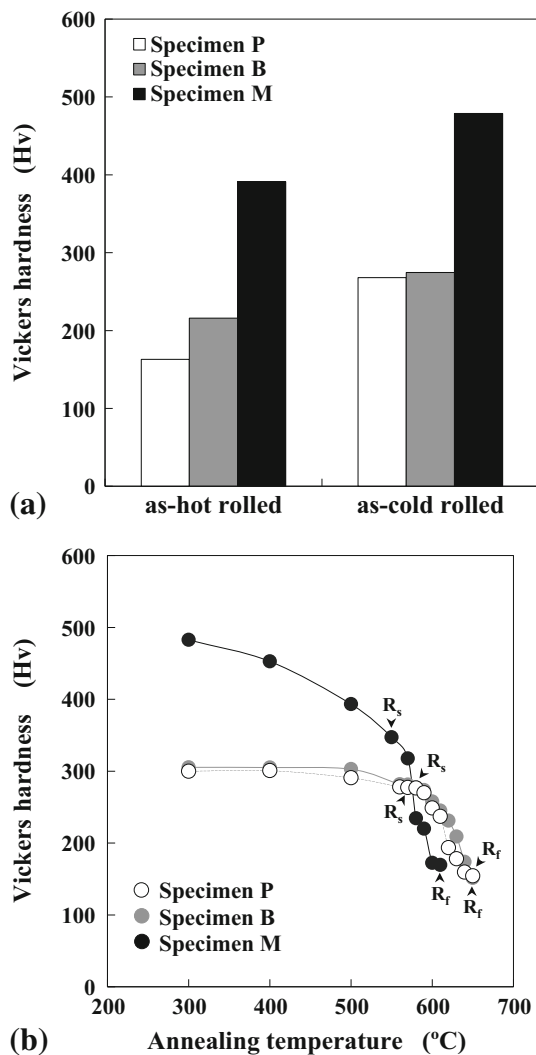
Fig. 6 (a) Vickers hardness of as-hot rolled and as-cold rolled sheets and (b) variation in Vickers hardness during heating (R_s: starting temperature of recrystallization, R_f: finishing temperature of recrystallization)

Fig. 7 (a) IQ, (b) ND, and (c) RD orientation maps for specimen M immediately before start of ferrite recrystallization

of each specimen annealed at 610 °C is shown in Fig. 4. Recrystallization of ferrite was complete in specimen M (Fig. 4c), whereas many non-recrystallized ferrite grains were observed in specimens P and B (Fig. 4a and b, respectively). As shown in Fig. 4(a), it should be noted that recrystallized ferrite grains mainly nucleated at the interface between the ferrite regions and the pearlite colonies in specimen P. Figure 5 shows the ferrite grain size for each specimen immediately after the completion of ferrite recrystallization. The grain size decreased in the order of specimen B > P > M, and the grain size for specimen B was approximately 1.7 times larger than that for specimen M.

Vickers hardness of as-hot rolled and as-cold rolled sheets is shown in Fig. 6(a). Figure 6(b) shows the variation in Vickers hardness during heating from 300 °C to the finishing temperature for ferrite recrystallization. The hardness of specimen M decreased markedly during the recovery stage, while that of specimen P decreased only slightly, and that of specimen B hardly changed. When the temperature exceeded 500 °C, the

hardness of specimen B also decreased slightly. In addition, the hardness decreased markedly during the ferrite recrystallization stage in all specimens. Figure 7 shows an image quality (IQ) map and ND and rolling direction (RD) orientation maps for specimen M immediately before the start of ferrite recrystallization (starting temperature of ferrite recrystallization: 530 °C). In previous studies (Ref 10, 14), subgrains formed in non-recrystallized ferrite grains can be recognized as regions with very fine polygonal grains in the IQ maps. Moreover, non-recrystallized ferrite grains without the formation of clear subgrains can be recognized as regions with low IQ value, namely, dark regions, owing to its higher dislocation density. As shown in Fig. 7(a), a major portion of regions in the IQ map was relatively dark, and very fine polygonal grains were hardly observed. Therefore, very few clear subgrains were observed in specimen M immediately before the start of ferrite recrystallization, although the hardness decreased markedly during the recovery stage from 300 to 520 °C. Furthermore, there were non-recrystallized α grains with both γ-fiber and α-fiber (RD// <110>) regions (Fig. 7b and c).
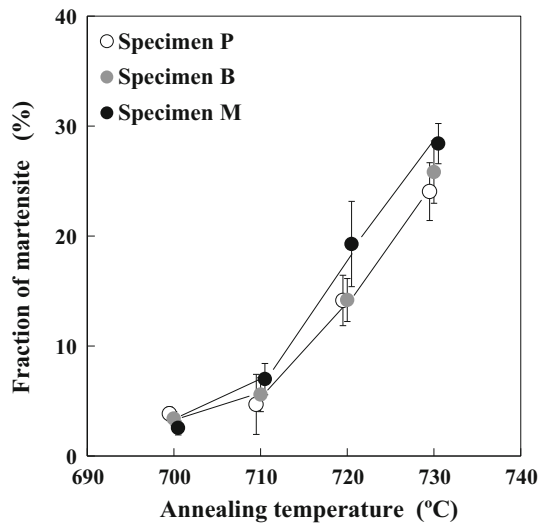
Fig. 8 Martensite fraction for specimens P, B, and M as function of annealing temperature

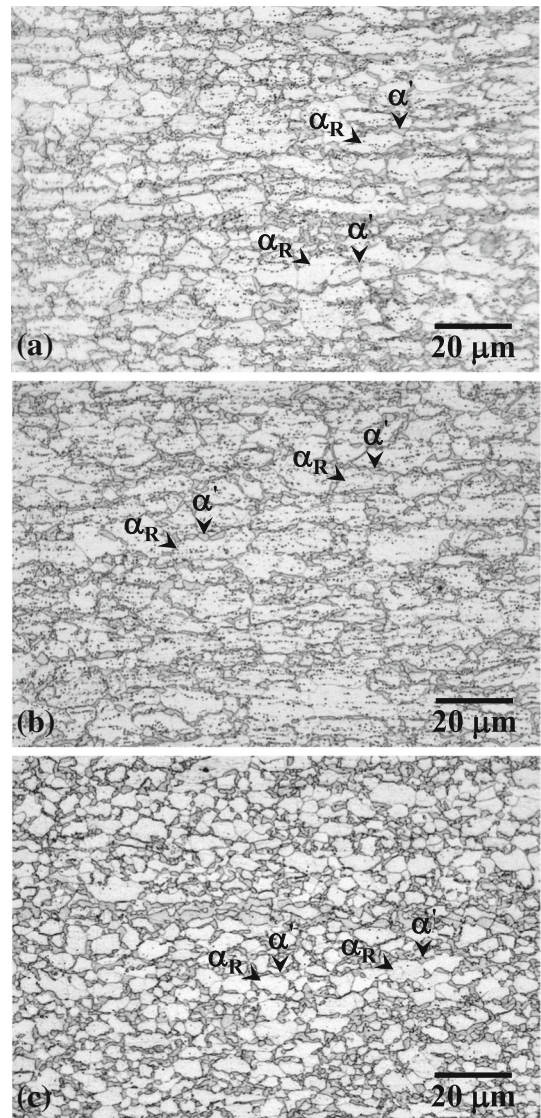### 3.2 Microstructural Evolution During Intercritical Annealing

Figure 8 shows the variation in the fraction of austenite, i.e., martensite, in each specimen annealed at intercritical temperatures. The fraction of martensite increased with increasing annealing temperature for all specimens, but was always largest for specimen M.

Figure 9 shows the microstructure of each specimen heated to 720 °C. As mentioned above, the recrystallization of ferrite was complete in all specimens when they were heated to intercritical temperatures. The spheroidal cementite was still present in specimens P and B (Fig. 9a and b), but scarcely so in specimen M (Fig. 9c). Furthermore, most of the martensite was formed at the recrystallized ferrite grain boundaries in all specimens. Figure 10 shows SEM images of the microstructure of each specimen annealed at 710 and 720 °C. Cementite particles were uniformly distributed in all specimens annealed at 710 °C (Fig. 10a-c), and were smallest in specimen M. The cementite particles in specimens P and B persisted through the annealing at 720 °C, whereas those in specimen M were almost completely dissolved (Fig. 10d-f).

The distribution of distance between martensite regions in the normal and rolling directions for each specimen heated to 720 °C is shown in Fig. 11. For specimens P and B, the distance between martensite regions varied widely in the normal and rolling directions. In contrast, the scatter was comparatively small for specimen M. Figure 12 shows the average distance between martensite regions in the normal and rolling directions for each specimen heated to 720 °C. In the case of specimens P and B, the distance between martensite regions in the rolling direction was much longer than that in the normal direction. On the contrary, the distance between martensite regions in the rolling direction was comparable to that in the normal direction for specimen M.

4. Discussion

One noteworthy finding of the present study is that microstructural evolution during annealing varied significantly
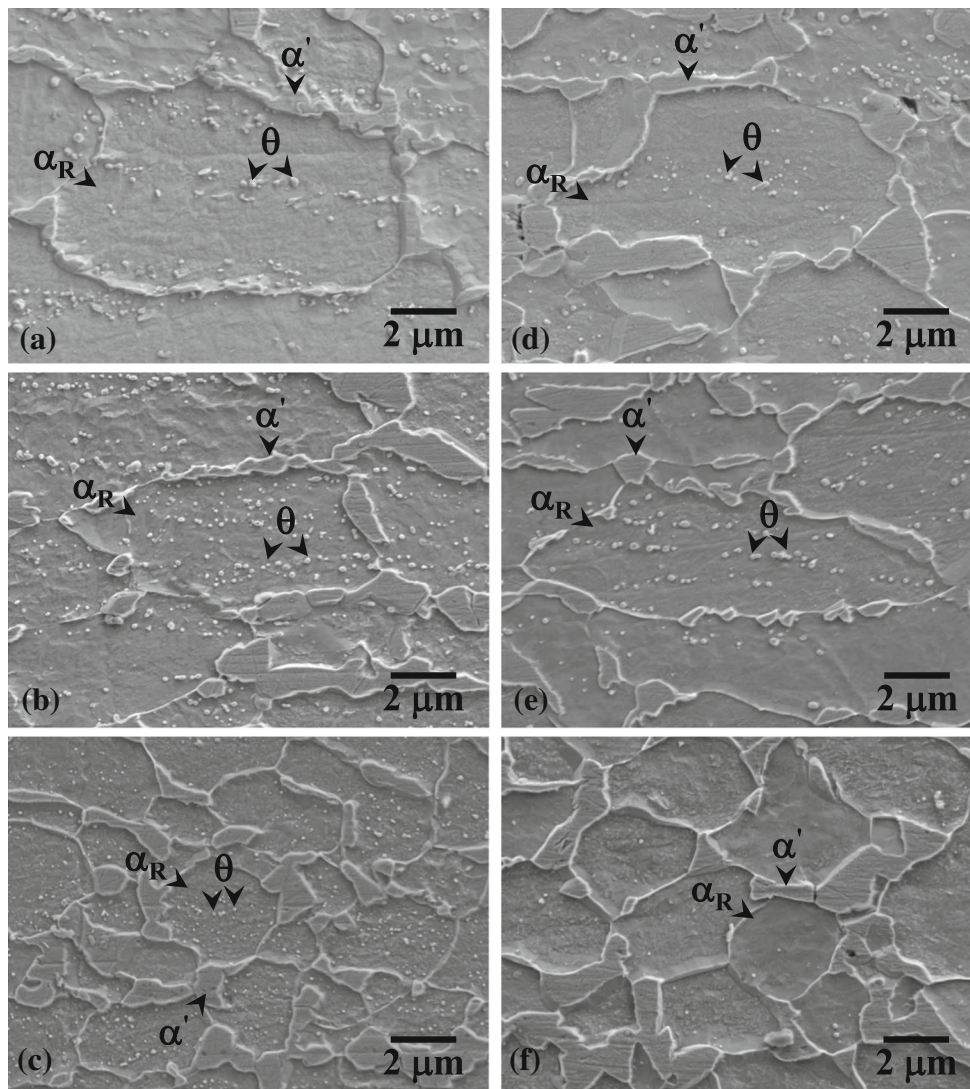

Fig. 9 Microstructure of specimens (a) P, (b) B, and (c) M, heated to 720 °C (α_R: recrystallized ferrite grains, α': martensite)

depending on the initial microstructure. Here, we discuss the microstructural evolution during annealing by focusing on the effect of the initial microstructure on the recovery and recrystallization of ferrite, and the ferrite-to-austenite phase transformation.

4.1 Effect of Initial Microstructure on Recovery and Recrystallization of Ferrite

As seen in Fig. 4, ferrite recrystallization was markedly more rapid in specimen M than in specimens P and B. Moreover, the decrease in hardness for specimen M during the recovery stage was much more significant than that for specimens P and B (Fig. 6). This explains why progress of recovery was more rapid and extensive in specimen M than in specimens P and B (Fig. 6). In general, the dislocation density in as-quenched martensite is extremely high; however, if the dislocations are distributed uniformly, the recrystallization do not occur even if the dislocation density is high (Ref 15). Moreover, Tokizane et al. (Ref 16) demonstrated that the

Fig. 10 SEM images of microstructure in specimens (a) P, (b) B, and (c) M, heated to 710 °C, and specimens (d) P, (e) B, and (f) M, heated to 720 °C (α_R: recrystallized ferrite grains, α': martensite, θ: cementite particles)

recrystallization of as-quenched lath martensite was not observed on tempering, whereas the deformed lath martensite easily recrystallized. Once martensite is cold rolled, a deformed structure that is non-uniform in terms of dislocation density and local crystal rotation is introduced (Ref 17), as also clearly revealed in Fig. 2(c) and 7(a). Thus, it is likely that progress of recovery and recrystallization of ferrite were markedly more rapid in martensite than in bainite or pearlite, because the dislocation density and its heterogeneity for specimen M after cold rolling was larger than that for specimens P and B. In a previous study (Ref 6), progress of ferrite recrystallization in low-carbon steel with an initial martensite-containing microstructure was found to be more rapid than that in low-carbon steel with ferrite and pearlite as the initial microstructure, which is consistent with the present results.

The recrystallized ferrite grains in specimen M were finer and more equiaxed than those in specimens P and B. In the case of Ti-containing low-carbon steel, it has been demonstrated that

equiaxed recrystallized ferrite grains are formed when recrystallization and subgrain growth occurs during annealing (Ref 14). However, as shown in Fig. 7(a), hardly any subgrains were observed in specimen M immediately before the onset of ferrite recrystallization. Ueji et al. (Ref 17) reported that ultrafine equiaxed ferrite grains were present in annealed low-carbon steel owing to non-uniform deformation during cold rolling of martensite. Takaki et al. (Ref 15) showed that cold rolling of lath martensitic steel caused the intrusion of slip bands into the matrix, resulting in an increase in the number of nucleation sites for ferrite recrystallization during annealing. Thus, the number of such nucleation sites in specimen M probably increased due to non-uniform deformation during cold rolling of martensite, leading to the formation of fine equiaxed recrystallized ferrite grains. Karmakar et al. (Ref 6) reported that fine recrystallized ferrite grains in low-carbon steel whose initial microstructure include martensite is attributable to grain-boundary pinning by fine cementite particles. As shown in Fig. 10, the spheroidal
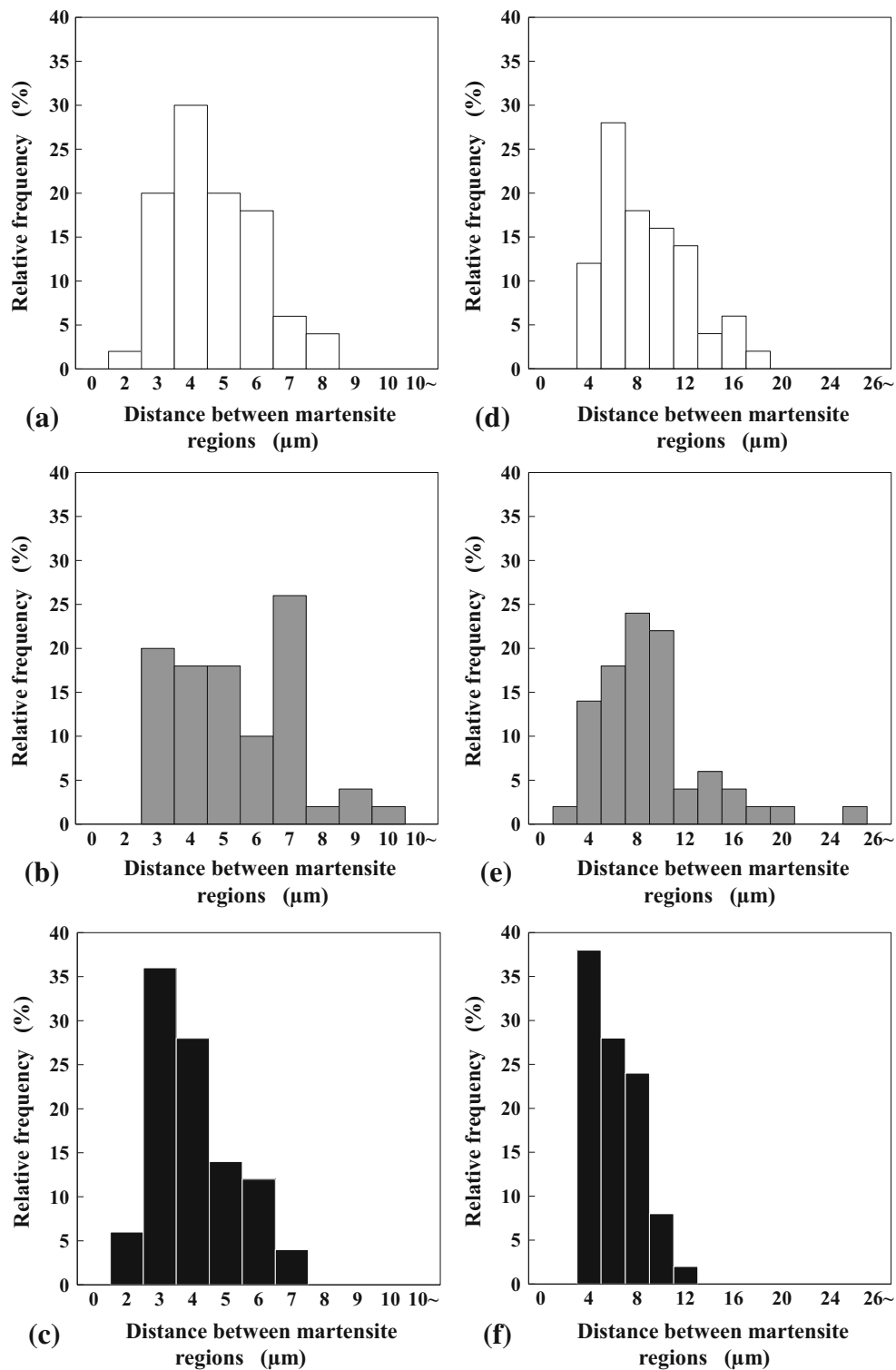
Fig. 11 Distribution of distance between martensite regions in normal direction for specimens (a) P, (b) B, and (c) M, and in rolling direction for specimens (d) P, (e) B, and (f) M, heated to 720 °C

cementite in specimen M was finer than that in specimens P and B. Accordingly, the formation of fine recrystallized ferrite grains might also be attributable to such pinning.

For the comparison between specimens P and B, the hardness of specimen P slightly decreased, while that of

specimen B hardly changed, during heating from 300 to 650 °C (the onset temperature of recrystallization). This indicates that progress of recovery in specimen P was slightly more rapid than that in specimen B. Furthermore, progress of ferrite recrystallization in specimen P was faster than that in specimen
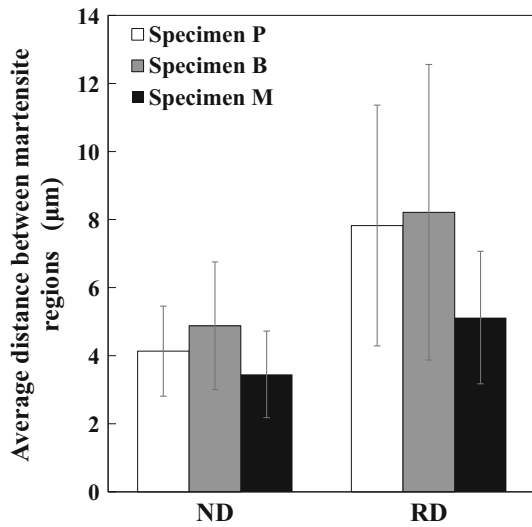
Fig. 12 Average distance between martensite regions in normal and rolling directions for specimens P, B, and M, heated to 720 °C

B (Fig. 4). It has been demonstrated that when an external stress is applied to ferrite-pearlite steel, cracks nucleate mainly at ferrite-pearlite interfaces, ferrite–ferrite grain boundaries, and within ferrite grains (Ref 18, 19). Narasaiah et al. (Ref 19) reported that ferrite-pearlite interfaces and ferrite–ferrite grain boundaries are preferred crack initiation sites compared with the interior of ferrite grains. These findings imply that the strain in ferrite-pearlite steel tends to concentrate at ferrite-pearlite interfaces and ferrite–ferrite grain boundaries, which is also likely to be the case in the present study. It is well known that the higher the geometrically necessary dislocation density is, the more accelerated recovery and recrystallization will be. As shown in Fig. 4(a), recrystallized ferrite grains nucleated at the interface between ferrite and pearlite in specimen P. Thus, the dislocation density at the interface between ferrite and pearlite in specimen P during cold-rolling may be larger than the average dislocation density in specimen B, and the strain concentration at the interface during cold-rolling may accelerate progress of recovery and recrystallization of ferrite in specimen P.

4.2 Effect of Initial Microstructure on Ferrite-to-Austenite Phase Transformation

As shown in Fig. 9, for all specimens, most of the martensite was formed at recrystallized ferrite grain boundaries. Therefore, the austenite nucleation sites during intercritical annealing were mainly at such boundaries. It has been showed that for the low-carbon steel, austenite nucleation sites are mainly at high-angle grain boundaries such as those between recrystallized ferrite grains, and low-angle grain boundaries such as subgrain boundaries (Ref 8, 10). Furthermore, it has been reported that austenite nucleation sites during intercritical annealing of low-carbon steel are mainly at pearlite colonies when the initial microstructure includes pearlite (Ref 13, 20, 21). However, for specimen P, very little such nucleation was

observed. Yang et al. (Ref 22) demonstrated that austenite forms in several stages, and nucleates primarily at ferrite–ferrite grain boundaries. Moreover, Huang et al. (Ref 13) reported that austenite nucleates at both recrystallized ferrite grain boundaries and pearlite colonies when the heating rate is low (1 °C/s). These findings indicate that austenite preferentially nucleates at recrystallized ferrite grain boundaries after the completion of ferrite recrystallization. Accordingly, it appears that the distribution of martensite (austenite during intercritical annealing) depends on the morphology of the recrystallized ferrite grains. As shown in Fig. 5, 11, and 12, the distribution of martensite in specimen M with equiaxed ferrite grains was relatively uniform. In contrast, that in specimens P and B with elongated ferrite grains was non-uniform. These results suggest that controlling the morphology of recrystallized ferrite grains is very important in order to form a uniform martensite distribution.

The distribution of martensite was almost the same in specimens P and B (Fig. 11 and 12). This indicates that the austenite nucleation sites were mainly at recrystallized ferrite grain boundaries since the morphology and size of these grains were almost the same in both specimens. On the other hand, it has been reported that austenite forms at cementite particles when the heating rate is high (Ref 6, 13), and the cementite particles in specimen B were uniformly distributed before the start of ferrite recrystallization (Fig. 10b and e). Thus, the influence of the distribution of cementite particles before annealing on the distribution of martensite is presumably small at a heating rate of 0.5 °C/s.

As seen in Fig. 8, the fraction of martensite in specimen M was larger than that in specimens P and B at all temperatures. As described above, the austenite nucleation sites were mainly at high-angle grain boundaries such as those between recrystallized ferrite grains. Thus, it is likely that the number of austenite nucleation sites was larger in specimen M than in specimens P and B, since the grain size was smaller in specimen M. It has been reported that the increase in the austenite fraction during intercritical annealing is caused by an increase in the number of austenite nucleation sites (Ref 10). Thus, the high martensite fraction in specimen M was presumably caused by the large number of austenite nucleation sites caused by grain refinement of ferrite.

The results in Fig. 10 clearly indicate that cementite dissolution was more rapid in specimen M than in specimens P and B. It has been reported that the surface energy for cementite particles increases as the particle size decreases, thereby accelerating cementite dissolution (Ref 23). As shown in Fig. 10, the cementite particles in specimen M were smaller than those in specimens P and B. Thus, cementite dissolution in specimen M was likely accelerated.

Figure 13 illustrates the microstructural evolution that occurs during annealing for each specimen. As described above, control of ferrite recrystallization during annealing is the most important factor determining the distribution of martensite at low heating rates. The results of the present study suggest that the presence of equiaxed fine ferrite grains plays a very important role in forming a uniform microstructure in low-carbon steels.
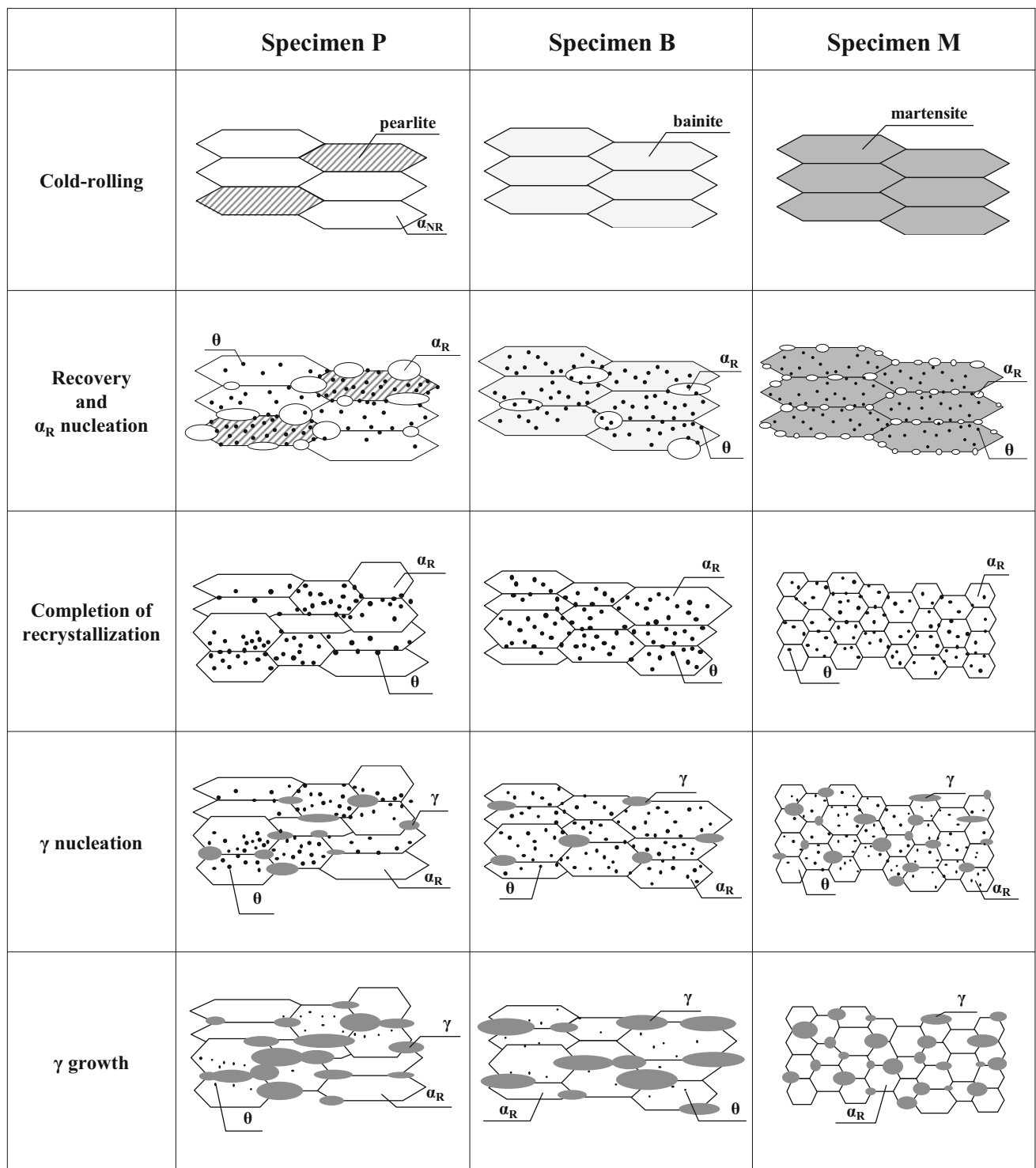
Fig. 13 Schematics showing microstructural evolution during annealing for each specimen (α_{NR}: non-recrystallized ferrite, α_R: recrystallized ferrite, θ: cementite, γ: austenite)

5. Conclusions

Microstructural evolution during cold rolling and subsequent annealing of low-carbon steel with different initial microstructures was investigated from the perspective of the competitive phenomenon between recrystallization of ferrite and reverse phase transformation from ferrite to austenite, and the following results were obtained.

1. Progress of recovery and recrystallization of ferrite in specimen M (martensite) was markedly more rapid than that in specimens P (pearlite) and B (bainite), owing to the non-uniform microstructure and high dislocation density in specimen M. Furthermore, the recrystallized ferrite grains in specimen M were finer and more equiaxed than those in specimens P and B.

2. Progress of recovery and recrystallization of ferrite in specimen P was slightly more rapid than that in specimen B, owing to preferential nucleation of recrystallized ferrite grains at the interface between the ferrite regions and the pearlite colonies.

3. In all specimens, the main austenite nucleation sites were high-angle grain boundaries such as those between recrystallized ferrite grains. In addition, the fraction of pearlite colonies in specimen P that became austenite nucleation sites was extremely low.

4. The martensite fraction in specimen M was larger than that in specimens P and B at all temperatures, owing to the increased number of austenite nucleation sites. Moreover, progress of cementite dissolution was more rapid in specimen M than in specimens P and B.

As mentioned above, the recovery and recrystallization behaviors are different due to the initial microstructures, and the difference of recovery and recrystallization behavior can affect the ferrite-to-austenite phase transformation behavior (especially austenite fraction during intercritical annealing).

References

1. M. Abe, Y. Koyabu, Y. Hayashi, and S. Hayami, Effect of Grain Boundaries on the Cold Rolling and Annealing Textures of Pure Iron, *Trans. Jpn. Inst. Met.*, 1982, **23**, p 718–725

2. T. Senuma and M. Kameda, Influence of Grain Refinement of Hot Band on Rolling and Recrystallization Textures of Plain Extra Low Carbon Steel Sheets, *J. Jpn. Inst. Met. Mater.*, 1996, **60**, p 717–726 (in Japanese)

3. T. Nakamura, T. Fukutsuka, and Y. Yagi, Cold Rolling and Recrystallization Textures of High-Purity Iron, *Tetsu-to-Hagané*, 1972, **58**, p 2025–2033 (in Japanese)

4. S. Uchida, I. Sawai, and E. Kamisaka, Influence of Hot Rolled Microstructure on the Recrystallization at Surface Layer of Cold Rolled Low Carbon Steel Sheets, *Tetsu-to-Hagané*, 1984, **70**, p 2144–2151 (in Japanese)

5. H.C. Chen, K. Tomokiyo, H. Era, and M. Shimizu, Effect of Microstructure in Hot Rolled Steel on the Formation of Retained Austenite and Mechanical Properties in Cold Rolled and Annealed Steel Sheet, *Tetsu-to-Hagané*, 1989, **75**, p 626–633 (in Japanese)

6. A. Karmakar, M. Ghosh, and D. Chakrabarti, Cold-Rolling and Intercritical Annealing of Low-Carbon Steel: Effect of Initial Microstructure and Heating-Rate, *Mater. Sci. Eng. A*, 2013, **564**, p 389–399

7. N. Maruyama, T. Ogawa, and M. Takahashi, Recrystallisation at Intercritical Annealing in Low Carbon Steel, *Mater. Sci. Forum*, 2007, **558–559**, p 247–252

8. T. Ogawa, N. Maruyama, N. Sugiura, and N. Yoshinaga, Incomplete Recrystallization and Subsequent Microstructural Evolution During Intercritical Annealing in Cold-Rolled Low Carbon Steels, *ISIJ Int.*, 2010, **50**, p 469–475

9. T. Ogawa, N. Sugiura, N. Maruyama, and N. Yoshinaga, Influence of State of Nb on Recrystallization Temperature During Annealing in Cold-Rolled Low-Carbon Steels, *Mater. Sci. Eng. A*, 2013, **564**, p 42–45

10. T. Ogawa, K. Sato, H. Dannoshita, K. Maruoka, and K. Ushioda, Role of Nb on Microstructural Evolution During Intercritical Annealing in Low-Carbon Steels, *ISIJ Int.*, 2016, **56**, p 2290–2297

11. T. Nonaka, N. Fujita, H. Taniguchi, T. Tomokiyo, and K. Goto, Development of Ultra-high-Strength Steel Sheets With Excellent Formabilities, *Mater. Jpn.*, 2007, **46**, p 108–110 (in Japanese)

12. T. Ono, T. Hosomi, Y. Takemoto, and T. Senuma, Influence of Various Factors on the Refinement of Martensitic Microstructures of Hot Stamped Steel Components, *Tetsu-to-Hagané*, 2013, **99**, p 475–483 (in Japanese)

13. J. Huang, W.J. Poole, and M. Militzer, Austenite Formation During Intercritical Annealing, *Metal. Mater. Trans. A*, 2004, **35**, p 3363–3375

14. N. Sugiura, N. Yoshinaga, K. Kawasaki, Y. Yamaguchi, J. Takahashi, and T. Yamada, Influence of Solute C on Recrystallization Behavior in Ti Added Low Carbon Cold Rolled Sheet Steel, *Tetsu-to-Hagané*, 2008, **94**, p 179–187 (in Japanese)

15. S. Takaki, S. Iizuka, K. Tomimura, and Y. Tokunaga, Influence of Cold Working on Recovery and Recrystallization of Lath Martensite in 0.2% C Steel, *J. Jpn. Inst. Met. Mater.*, 1991, **55**, p 1151–1158 (in Japanese)

16. M. Tokizane, N. Matsumura, K. Tsuzaki, T. Maki, and I. Tamura, Recrystallization and Formation of Austenite in Deformed Lath Martensitic Structure of Low Carbon Steels, *Metall. Trans. A*, 1982, **13A**, p 1379–1388

17. R. Ueji, N. Tsuji, Y. Minamino, and Y. Koizumi, Ultragrain Refinement of Plain Low Carbon Steel by Cold-Rolling and Annealing of Martensite, *Acta Mater.*, 2002, **50**, p 4177–4189

18. H. Yaguchi, T. Tsuchida, Y. Matsushima, S. Abe, K. Iwasaki, and A. Inada, Effect of Microstructures on the Fatigue Behavior of V-Added Ferrite-Pearlite Type Microalloyed Steels, *Kobe Steel Eng. Rep.*, 2000, **50**, p 53–56 (in Japanese)

19. N. Narasaiah and K.K. Ray, Small Crack Formation in a Low Carbon Steel with Banded Ferrite-Pearlite Structure, *Mater. Sci. Eng. A*, 2005, **392**, p 269–277

20. G.R. Speich, V.A. Demarest, and R.L. Miller, Formation of Austenite During Intercritical Annealing of Dual Phase Steels, *Metal. Trans. A*, 1981, **12**, p 1419–1428

21. W.C. Jeong and C.H. Kim, Formation of Austenite from a Ferrite-Pearlite Microstructure During Intercritical Annealing, *J. Mater. Sci.*, 1985, **20**, p 4392–4398

22. D.Z. Yang, E.L. Brown, D.K. Matlock, and G. Krauss, Ferrite Recrystallization and Austenite Formation in Cold-Rolled Intercritically Annealed Steel, *Metall. Trans. A*, 1984, **16A**, p 1385–1392

23. H. Sueyoshi, K. Suenaga, and R. Tanaka, Effect of Austenitizing Treatment Following by Slow Cooling on Graphitization in Hypoeutectoid Alloy Steels, *J. Jpn. Inst. Met. Mater.*, 1987, **51**, p 518–524 (in Japanese)